 DOI: 10.1002/mawe.200700263

Comparison between RVE and full mesh approaches for the simulation of compression tests on cellular metals

Vergleich zwischen dem Einheitszellen-basierenden und dem vollständigen Netz-Ansatz zur Simulation des Druckversuchs zellularer Metalle

B. F. Oliveira[1], L. A. B. Cunda[2], A. Öchsner[3], G. J. Creus[1]

Metal foams are materials of recent development and application that show interesting combinations of physical and mechanical properties. Many applications are envisaged for such materials, particularly in equipments of passive safety, because of their high capacity of energy absorption under impact conditions. The damage analysis in metallic foams is a complex problem and must be performed in a finite strain context. Considering that compression is the dominant loading in impact situations, a finite deformation simulation including damage effects of a compression test on a cellular metal sample is shown in this work. The main objective of the paper is to compare simulations considering periodic boundary conditions, by means of a representative volume element (RVE) approach, with results obtained using full meshes. It is shown that, when the imposed deformation is high, the use of RVE does not describe in a proper manner the deformation that occurs at the walls of cells. This characteristic of RVE approach results in a too stiff behavior when considering load-displacement relations. A comparison with experimental results is also presented.

Keywords: Cellular Metals; Metallic Foams; Damage; Gurson Models; Finite Elements

Schlüsselworte: Zellulare Metalle; metallischer Schaum; Schädigung; Gurson Modell; Finite Elemente

1 Introduction

This work continues the research on the simulation of metallic foams behavior that was presented in earlier papers [1, 2, 3].

We understand by metal foam a material composed by a metallic matrix with internal voids (*Fig. 1*). Metallic foams are increasingly considered by the automotive industry, particularly as recourse of passive safety. In that case, they act to absorb impact energy.

Metallic foams show mechanical behavior and physical properties that strongly differ from those of solid materials and show interesting combinations of properties. For example, high stiffness combined with low specific weight, or permeability to gas flow combined with high thermal conductivity, offering possibilities of use in aerospace and automotive industries. The schematic stress-strain curve for a metallic foam in compression (*Fig. 2*), shows a large area in the plateau region corresponding to high energy absorption at constant stress.

In order to employ these materials as a main component in protection structures, it is necessary to have reliable numerical methods and constitutive relations, developed and validated using experimental procedures that take into account the variety of mechanical, geometrical and physical properties of the foam and the base material.

2 Gurson damage model

The Gurson damage model was developed to describe the mechanical effect of high plastic deformations in ductile metals. The loss of resistance is governed by the porosity level. The (isotropic) damage variable employed is the volumetric void fraction, represented by f and defined by $f = V_v / V$, where V_v is the volume of voids in a representative small volume V, corrected for effects as stress concentration, etc.; f is defined at each point of the continuum. The presence of voids alters the elastoplastic constitutive relations. The equations usually employed in computational damage analyses, the Gurson-Tvergaard model [5, 6], considers a yield surface defined by

$$\Phi = \sqrt{\frac{3}{2} S_{ij} S_{ij}} - \overline{\omega} \sigma_y = 0 \qquad (1)$$

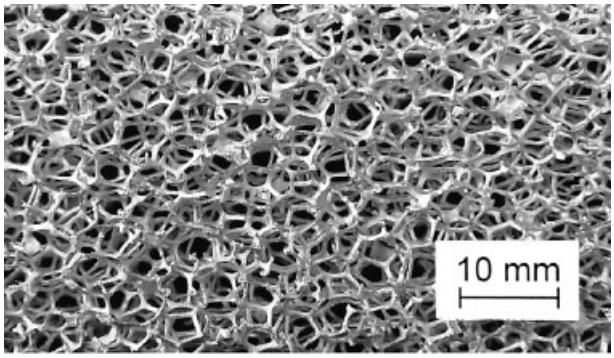

Fig. 1. Aluminum foam with open cell (DUOCEL®), [3].
Abb. 1. Offenzelliger Aluminium-Schaum (DUOCEL®), [3].

[1] Federal University of Rio Grande do Sul
[2] Federal University of Rio Grande
[3] Technical University of Malaysia

where

$$\overline{\omega} = \left[1 - 2\alpha_1 f \cosh\left(\frac{\alpha_2 3p}{2\sigma_y}\right) + \alpha_3 f^2\right]^{1/2} \tag{2}$$

$$S_{ij} = \sigma_{ij} - p\delta_{ij} \qquad p = 1/3\sigma_{ij}\delta_{ij} \tag{3}$$

$$\alpha_1 = \frac{1}{f_U} = 1.5 \qquad \alpha_2 = 1.0 \qquad \alpha_3 = \alpha_1^2 \tag{4}$$

and σ_{ij} are the Cauchy stresses, σ_y the yield stress in simple tension. α_i are material parameters. The parameter $f_U = 1/\alpha_1$ is the maximum volumetric void fraction admissible before rupture in the absence of pressure. Another possible interpretation for the α_1 and α_2 parameters is that they work as multipliers acting on porosity f and pressure p, respectively.

In *Fig. 3*, yield surfaces for different levels of void content are shown, in a plot of normalized deviatoric stress versus normalized pressure.

It can be seen that the plastic domain depends on the hydrostatic pressure. When the volumetric void fraction f decreases, decreases the influence of pressure, leading to a larger elastic domain. For $f = 0$, the model reduces to the von Mises model, which is independent of hydrostatic pressure. It should be noted here that in the absence of hydrostatic pressure, the coefficient $\overline{\omega}$ reduces to

$$\overline{\omega} = 1 - \alpha_1 f = 1 - \frac{f}{f_U} \tag{5}$$

The plastic strain rate tensor is given by,

$$D_{ij}^p = \dot{\lambda}\frac{\partial \Phi}{\partial \sigma_{ij}} \tag{6}$$

and the equivalent plastic strain rate is defined by

$$\dot{\varepsilon}^p = \sqrt{2}/_3 D_{ij}^p D_{ij}^p \tag{7}$$

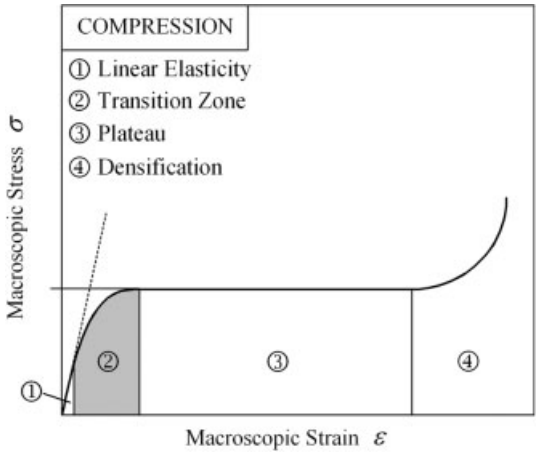

Fig. 2. Stress-strain curve for a metallic foam showing large capacity of energy absorption at constant stress, [4].

Abb. 2. Spannungs-Dehnungs-Kurve eines metallischen Schaums mit hohem Energieabsorptionsvermögen bei konstanter Spannung, [4].

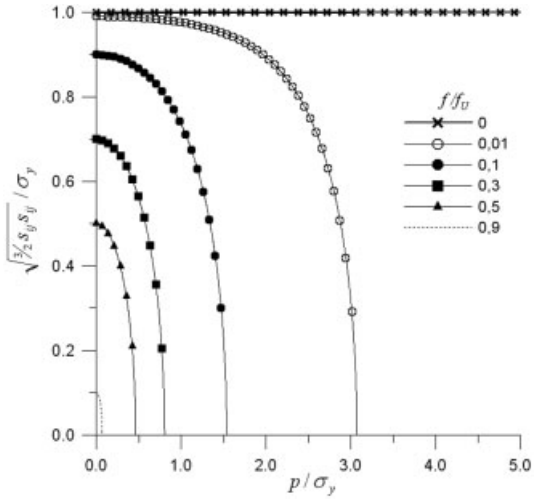

Fig. 3. Yield surface for a porous material: influence of volumetric void fraction.

Abb. 3. Fließfläche eines porösen Materials: Einfluss des volumetrischen Porenanteils.

The basic mechanisms of damage evolution are nucleation, growth and coalescence of voids. Nucleation occurs mainly due to material defects, in the presence of tension. Growth occurs when the voids (preexistent or nucleated) change their size according to the volume change in the continuum.

Coalescence is related to the fast rupture process that occurs after that the volumetric void fraction reaches a limit, indicated by f_C. Coalescence consists in the union of neighbor voids due to the rupture of a ligament.

The equations that govern damage evolution are modeled in a simplified form as follows. First, it is assumed that total void rate is given by

$$\dot{f}\begin{cases} \dot{f}_n + \dot{f}_g & f \le f_C \\ \dot{f}_c & f > f_C \end{cases} \tag{8}$$

where $\dot{f}_n$ is the void nucleation rate, $\dot{f}_g$ is the void growth rate and f_C is the void coalescence rate. Thus, as long as f is smaller than a characteristic value f_C, only nucleation and growth develop. Above f_C, only coalescence takes place.

The nucleation rate is proportional to the rate of equivalent plastic strain

$$\dot{f}_n = A(\varepsilon^p)\dot{\varepsilon}^p \tag{9}$$

For $A(\varepsilon^p)\dot{\varepsilon}^p$ Chu and Needleman [7] propose the statistical distribution

$$A(\varepsilon^p) = \frac{f_N}{S_N\sqrt{2\pi}}\exp\left[-\frac{1}{2}\left(\frac{\varepsilon^p - \varepsilon_N}{S_N}\right)^2\right] \tag{10}$$

where f_N, is the nucleation void volumetric fraction, ε_N is the plastic strain value for nucleation and S_N is the standard deviation for the distribution. Sometimes it is assumed that nucleation takes place only in tension [8,9], what implies that

$$A(\varepsilon^p) = 0 \qquad \text{if} \qquad p < 0 \tag{11}$$

Growth rate of voids is controlled by mass conservation through the expression

$$\dot{f}_g = (1 - f)D^p_{ii} \tag{12}$$

Voids increase or decrease their volume according to the volume variation in the continuum. Coalescence is governed [10] by the relation

$$\dot{f}_c = \frac{f_U - f_C}{\Delta\varepsilon}\,\dot{\varepsilon}^p \tag{13}$$

or in an alternative way [8, 11] employing in Eq. (2) a corrected volumetric void fraction given by

$$f^* = \begin{cases} f & f < f_C \\ f_C + \frac{(1.0 - f_C)}{(f_F - f_C)}(f - f_C) & f > f_C \end{cases} \tag{14}$$

In this case, only nucleation and growth are considered in Eq. (8).

The commercial finite element code ABAQUS is used in this work and the Gurson damage model is one of the available constitutive relationships.

3 Modeling considerations for metallic foams

Metal foam properties can change along the production process, particularly according to the cell being open or closed and the relative density of the foam in relation to the base material.

Moreover, foams show (Fig. 1) a fairly random structure. It is possible to determine the exact geometry using CT-scan (computer tomography) and model it with a dense mesh of finite elements, as in *Fig. 4*a. A different approach towards the understanding and modeling of these materials, adopted in this work, is an idealization as a cellular material with regular structure, as in Fig. 4b. In this case, modeling a RVE (representative volume element, Fig. 4c) and still considering the existent symmetries, good results can be obtained with fewer elements. Then, specimens with regular structure may be tested to validate results and determine material parameters. These homogenization procedures have been used with success in other areas of continuum mechanics. *Figure 5* shows a specimen of a cellular metal made to represent a foam.

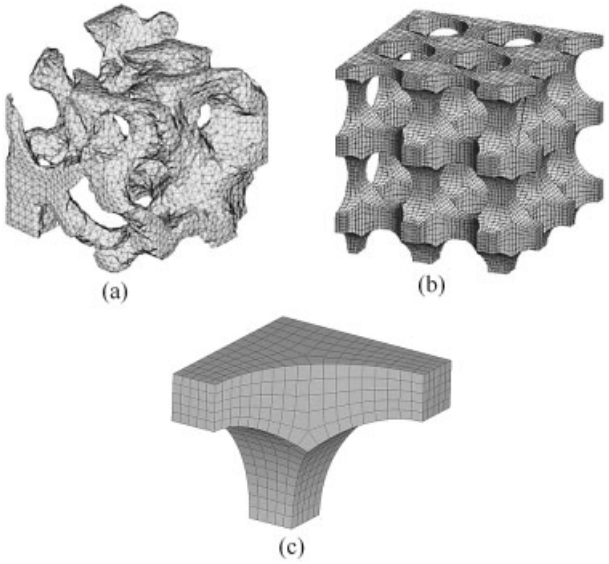

Fig. 4. Meshes used to represent a cellular metal, [3].
Abb. 4. Netze zur Darstellung eines zellularen Metalls, [3].

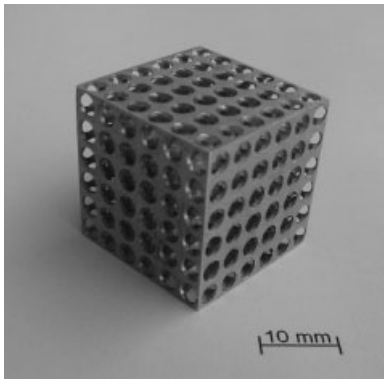

Fig. 5. Cube of cellular metal.
Abb. 5. Würfel eines zellularen Metalls.

3.1 Application of boundary conditions

One important aspect to take into account when modeling cells as those described above are the boundary conditions, that must represent the average behavior of the foam. When a vertical displacement is applied to the top side (*Fig. 6*) the vertical faces must continue vertical while the distance between them may change.

This behavior can be computationally imposed using multiple point constraints (MPC). The used FE code (ABAQUS) offers the possibility to realize such a boundary condition where all nodes on a certain surface have the same *x*-displacement: $u_{xi} = \ldots = u_{xj}$. The effect of differing boundary conditions on the deformation is shown in Fig. 6.

4 Simulation of a compression test on a cube of cellular metal

A cube of a cellular metal as shown in Fig. 5 is considered in the following. The cube contains 3 mm diameter holes with distance of 4 mm among them. The presence of holes simulates a cellular metal with relative density of 0.2712.

The matrix material properties are E = 72.7 GPa, ν = 0.34, initial yield value σ_y^0 MPa = 250 MPa and final yield value σ_y^∞ MPa = 410 MPa. Hardening is taken into account by the re-

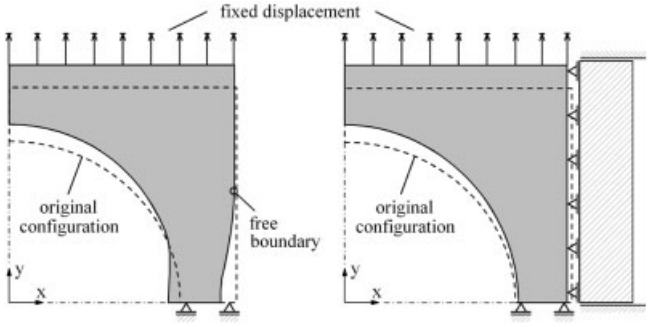

Fig. 6. Results of different boundary conditions applied to the right face, [3].
Abb. 6. Ergebnisse verschiedener Randbedingungen, die an der rechten Seite angewandt wurden, [3].

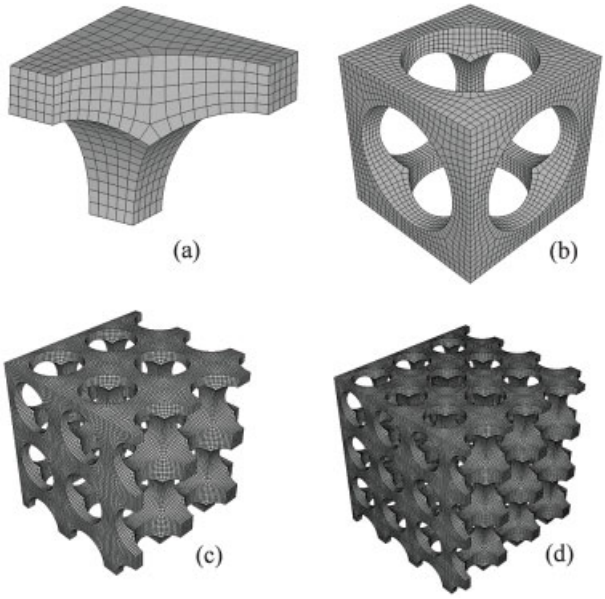

Fig. 7. Meshes used to study the cube. a) unit cell b) 2-cells c) 5-cells d) 7-cells.

Abb. 7. Netze zur Untersuchung des Würfels. a) Einheitszelle b) 2 Zellen c) 5 Zellen d) 7 Zellen.

lation $\sigma_y = \sigma_y^0 + (\sigma_y^\infty - \sigma_y^0)[1 - \exp(-k\varepsilon^p)]$, with $k = 25$. The Gurson model ABAQUS code is used and the parameters considered are 5 % of initial porosity, α_1 = 1.5 and α_2 = 1.0. The material parameters are obtained fitting experimental results [3, 12].

Load is applied as a vertical displacement on the top surface of the cube.

The objective of this analysis is to compare numerical results with experimental results available from a cellular metal cube compression tests, and to check if MPC boundary condition works properly in compression as in tension situations [1, 3].

Five models are used to simulate the problem, beginning with a single cell as shown in *Fig. 7*a, and varying the number of cells in each direction and the boundary conditions. The single cell model of Fig. 7a is studied with and without MPC boundary condition (see Fig. 6). With 2 cells in each direction the model called 2-cells (Fig. 7b) is obtained, representing a cube with a hole. Employing 5 or 7 cells in each direction the models called 5-cells (Fig. 7c) and 7-cells (Fig. 7d) are obtained.

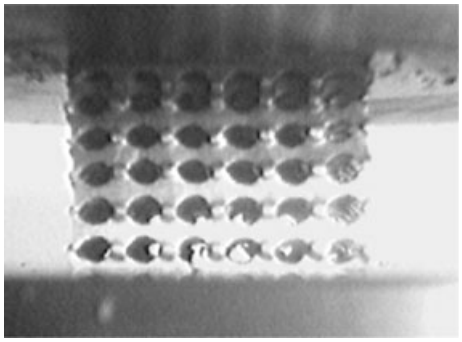

Fig. 9. Picture showing buckling process at the walls between holes.

Abb. 9. Darstellung des Beulverhaltens der Zellwände zwischen den Löchern.

Figure 8 shows a comparison among macroscopic stress and strain plots for the five models used in the analysis. The macroscopic stress is the relation between the resultant forces and the original solid surface area. The macroscopic strain is the ratio between change of length and original length. It can be seen that a unit cell (Fig. 7a) with MPC overestimates the stiffness of the model. Using MPC, due to the nature of the restriction (see section 3.1), the walls remain vertical. This effect is more significant after 2.5 % macroscopic strain, when buckling occurs in the walls between the holes (*Fig. 9*). *Figure 10* shows the von Mises stress distribution for the unit cell with MPC at an applied macroscopic strain of 25 %.

The 2-cells model (Fig. 7b) and a unit cell without MPC that represents an eighth of the 2-cells model, underestimate the stiffness of the cube because in this case all the walls suffer strong buckling effects, that in the actual behavior of the real specimen (Fig. 5) is restricted (at this loading level) to the slenderer external walls. *Figure 11* shows the von Mises stress distribution for the unit cell without MPC and *Fig. 12* and *13*, for the 2-cells model. In both cases for an applied macroscopic strain of 25 %. In the figures the axe is 3 defines the load direction.

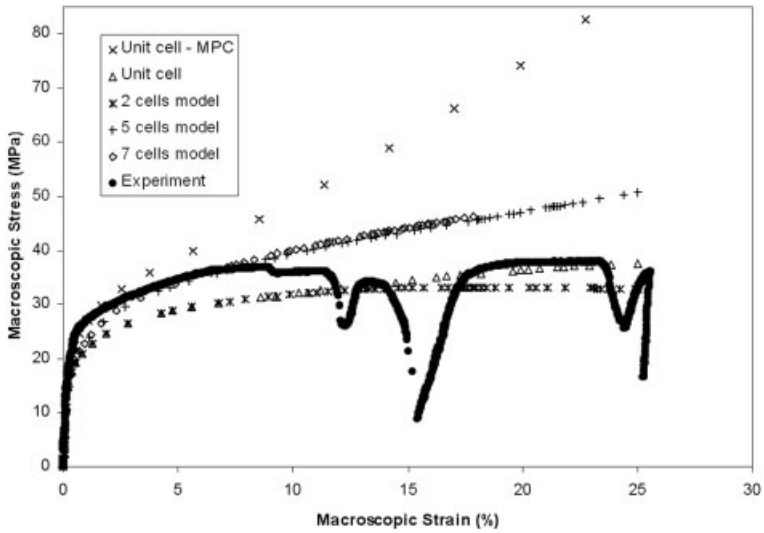

Fig. 8. Stress strain plots for the five models used in the analyses.

Abb. 8. Spannungs-Dehnungs-Diagramme der fünf verwendeten Modelle.

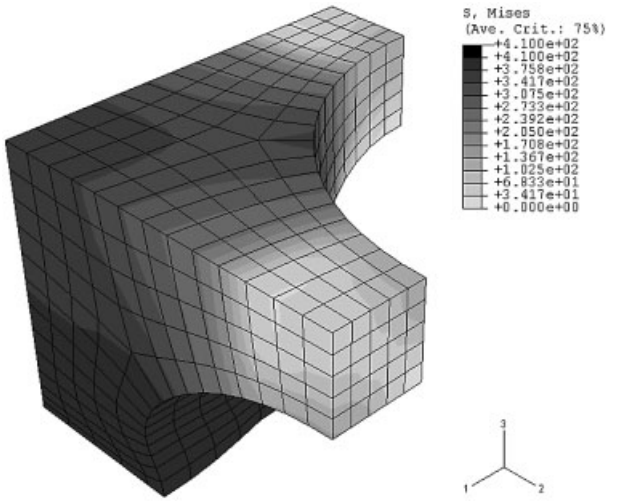

Fig. 10. Distribution of von Mises stress (MPa) for a unit cell with MPC for an applied macroscopic strain of 25 %.

Abb. 10. Verteilung der von Mises Spannung (MPa) in einer Einheitszelle mit MPC bei einer makroskopischen Dehnung von 25 %.

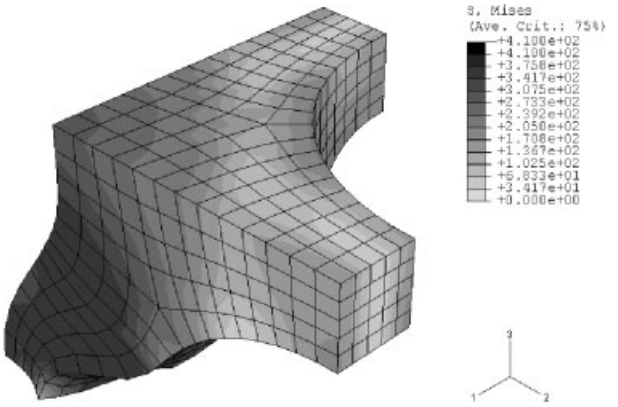

Fig. 11. Distribution of von Mises stress (MPa) for a unit cell without MPC for an applied macroscopic strain of 25 %.

Abb. 11. Verteilung der von Mises Spannung (MPa) in einer Einheitszelle ohne MPC bei einer makroskopischen Dehnung von 25 %.

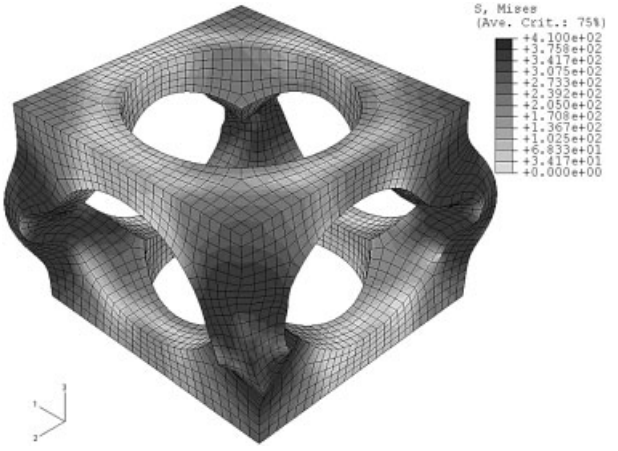

Fig. 12. Distribution of von Mises stress (MPa) for the 2-cells model for an applied macroscopic strain of 25 % - panoramic view.

Abb. 12. Verteilung der von Mises Spannung (MPa) in einem Modell mit zwei Zellen bei einer makroskopischen Dehnung von 25 % - Panoramaansicht.

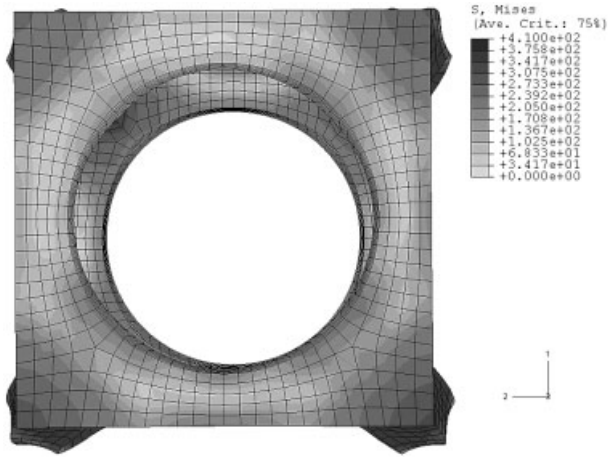

Fig. 13. Distribution of von Mises stress (MPa) for the 2-cells model for an applied macroscopic strain of 25 % - top view.

Abb. 13. Verteilung der von Mises Spannung (MPa) in einem Modell mit zwei Zellen bei einer makroskopischen Dehnung von 25 % - Draufsicht.

It can be observed in Fig. 8 that for macroscopic strains larger than 12 % there is a divergence in the unit cell and the 2-cells model plots, that can be explained by the fact that the 2-cells model presents a shear strain global effect (Fig. 12 and 13) not found in the one eighth model (unit cell without MPC).

For the 7-cells and the 5-cells models, that represent more appropriately the effect of the buckling at the walls between holes, numerical results are closer to experimental results. The 7-cells model results are obtained only until an applied strain of 17.85 %, due time-machine limitations and to avoid interpenetrations, since self-contact is not being considered. The mesh for this model has 253820 elements. The results to 5-cells model, with a 92500 elements, are obtained until an applied strain of 25 %, Fig. 8.

Figures 14 and *15* show von Mises stress distribution to the 7-cells model at an applied strain of 17.85 % and *Fig. 16* and *17*, for the 5-cells model at an applied strain of 25 %. It is pos-

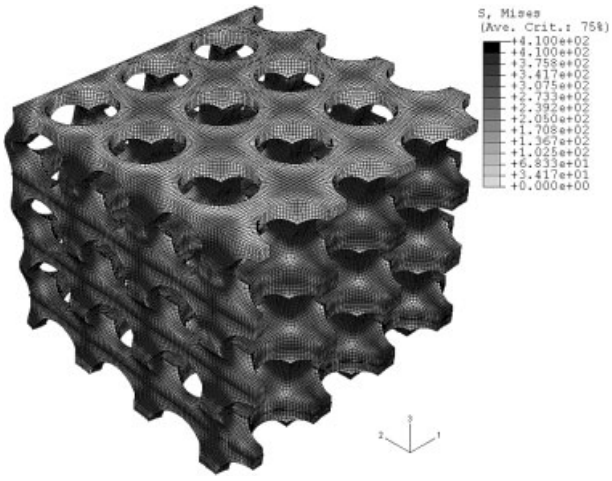

Fig. 14. Distribution of von Mises stress (MPa) for the 7-cells model for an applied macroscopic strain of 17.85 % - panoramic view.

Abb. 14. Verteilung der von Mises Spannung (MPa) in einem Modell mit sieben Zellen bei einer makroskopischen Dehnung von 17,85 % - Panoramaansicht.

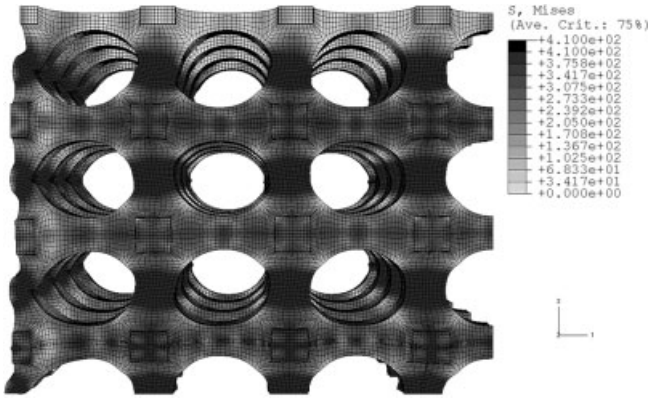

Fig. 15. Distribution of von Mises stress (MPa) for the 7-cells model for an applied macroscopic strain of 17.85 % - side view.

Abb. 15. Verteilung der von Mises Spannung (MPa) in einem Modell mit sieben Zellen bei einer makroskopischen Dehnung von 17,85 % - Seitenansicht.

sible to observe there that the buckling of the external walls is properly represented.

The experimental curve in Fig. 8 indicates how complex the real behavior is. After 12.8 % of the macroscopic strain there is a partial rupture with stiff decrease in load until a new equilibrium situation achieved by contact of the fragmented parts. This process repeats itself until the final failure.

5 Final comments

This paper presents some new results from a research in development ([1, 2]).

It is shown that MPC fails to represent the real behavior of the specimen in compression for large macroscopic strains (larger than 2.5 % in the present case), mainly due to buckling effects that are important at this strain level. The use of more complex models gives a good approximation of experimental results, up to a point close to postcritical softening (12.8 % in the present case). To represent the real behavior at much larger deformations, the introduction of self contact effects should be

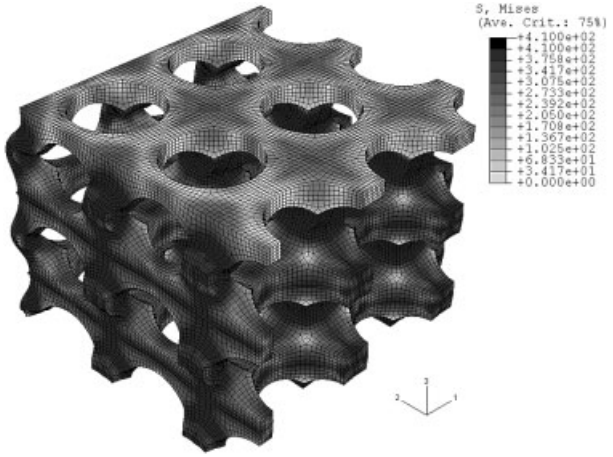

Fig. 16. Distribution of von Mises stress (MPa) for the 5-cells model for an applied macroscopic strain of 25 % - panoramic view.

Abb. 16. Verteilung der von Mises Spannung (MPa) in einem Modell mit fünf Zellen bei einer makroskopischen Dehnung von 25 % - Panoramaansicht.

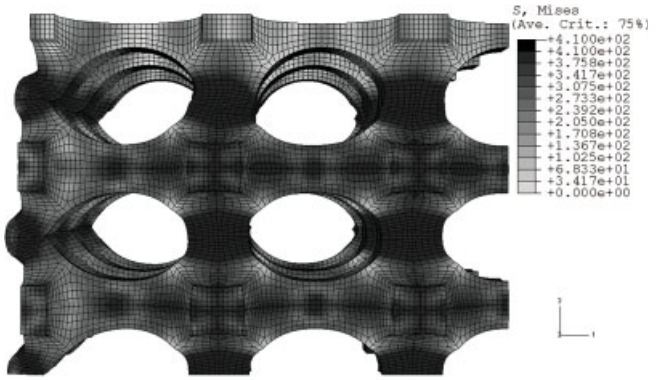

Fig. 17. Distribution of von Mises stress (MPa) for the 5-cells model for an applied macroscopic strain of 25 % - side view.

Abb. 17. Verteilung der von Mises Spannung (MPa) in einem Modell mit fünf Zellen bei einer makroskopischen Dehnung von 25 % - Seitenansicht.

needed. The research will continue looking for better models and damage parameters adjustment.

6 Acknowledgements

We thank CNPq, CAPES and GRICES for financial support though the CAPES/GRICES program (Proc. 127/05) and PROPESQ-UFRGS for continuous support of our research project.

7 References

1. B.F. Oliveira, L.A.B. Cunda, A. Öchsner, G.J. Creus, "Gurson damage model: applications to case studies", In: *Proceedings of the XXVII Iberian Latin-American Congress on Computational Methods in Engineering – CILAMCE 2006*, Brazil, September 3–6, **2006**.
2. L.A.B. Cunda, A. Öchsner, G.J. Creus, "Damage in metallic foams", In: Proceedings of the XXVI Iberian Latin-American Congress on Computational Methods in Engineering – CILAMCE 2005, Brazil, October 19–21, **2005**.
3. A. Öchsner, K. Lamprecht, *Mech. Res. Commun.* **2003**, *30*, 573.
4. A. Öchsner, W. Winter, G. Kuhn, *Arch. Appl. Mech.* **2003**, *73*, 261.
5. A.L. Gurson, *J. Eng. Mater.- T. ASME* **1977**, *99*, 2.
6. V. Tvergaard, *Int. J. Fracture* **1981**, *17*, 389.
7. C.C. Chu, A. Needleman, *J. Eng. Mater.- T. ASME* **1980**, *102*, 249.
8. ABAQUS, *Theory Manual v. 5.2,* Providence, USA: Hibbit, Karlsson & Sorensen, Inc., **1992**.
9. L.A.B. Cunda, G.J. Creus, *Comput. Model. Simul. Eng.* **1999,** *4*, 300.
10. V. Tvergaard, *Int. J. Solids Struct.* **1982**, *18*, 659.
11. V. Tvergaard, *Int. J. Fracture* **1981**, *17*, 389.
12. P. A. Munoz-Rojas, T. Fiedler, L.A.B. Cunda, A. Öchsner, G.J. Creus, "Parameter Identification to Simulate a Traction Test Applying Gurson Damage Model" In: *Proceedings of the CMNE 2007 – Congress on Numerical Methods in Engineering / CILAMCE 2007 - XXXVIII Latin-American Congress on Computational Methods in Engineering*, Porto, Portugal June 13–15, **2007**.

Corresponding author: Branca Freitas de Oliveira, Federal University of Rio Grande do Sul, Av. Osvaldo Aranha, 99, 4° andar, 90035–190, Porto Alegre, RS, Brasil, E-mail: branca@ufrgs.br

Received in final form: December 12, 2007 [T 263]